FRACTURE TOUGHNESS OF WOOD AND WOOD COMPOSITES DURING CRACK PROPAGATION

Noah Matsumoto
Structural Analysis Engineer - Methods and Allowables
Structures Technology
The Boeing Company
Mesa, AZ, USA

*John A. Nairn**†*
Professor and Richardson Chair
Wood Science & Engineering
Oregon State University
Corvallis, OR, USA

* Corresponding author: John.Nairn@oregonstate.edu
† SWST member

Fracture Toughness of Wood and Wood Composites During Crack Propagation

ABSTRACT

The mode I fracture toughness as a function of crack length of medium density fiberboard (MDF), particle board (PB), and Douglas-fir (DF) were all measured using a new energy-based method. PB and MDF are examples of composites that develop fiber bridging during crack propagation, which causes their toughness to increase with crack length. Longitudinal cracks in DF also displayed fiber bridging behavior, but only when the crack plane was normal to the tangential direction (TL cracks). MDF and PB experiments were done for both in-plane and out-of-plane cracks. The toughness of the former was much higher than the later. The in-plane crack toughness of MDF was higher then PB, but its out-of-plane toughness was lower. PB made using a new soy based resin had an in-plane toughness similar to commercial PB, but an out-of-plane toughness three times higher. Out-of-plane crack propagation is suggested as an improved method for measuring internal bond properties. When the fracture method was compared conventional internal bond (IB) tests, both methods showed that the soy PB is better, but the fracture method provided a clearer distinction.

Keywords: Fracture, Fiber Bridging, Numerical Modeling, R Curves, IB Tests

INTRODUCTION

Medium density fiberboard (MDF), particle board (PB) and Douglas-fir (DF) are three common building materials. MDF is composed of wood fibers commonly bonded together with a urea formaldehyde resin. PB is similar but made with wood particles, instead of fibers, and various resins, such as a recently-developed, formaldehyde-free soy based resin [Li *et al*. 2004]. DF is an important softwood species. Although DF is not a wood composite product, its internal biological structure makes it an anisotropic and heterogeneous material whose fracture properties are better studied with composite material fracture methods than with conventional fracture methods for isotropic, homogeneous materials.

Wood or wood composite structural performance is often assessed by bending strength tests (MOR) [ASTM 2009a] and internal bond tests (IB) [ASTM 2009b]. Experience in non-wood materials, however, suggests that fracture toughness is a better indicator of real-world performance than are strength tests [Williams 1984]. As such, fracture performance of wood and wood composites should be considered in wood design, but few tests are available.

A composites' fracture toughness comes from a number of sources, including its fiber or particles, their orientations, the resin or matrix, and the properties of the interfaces. Measuring the fracture toughness can be difficult in composites because they frequently develop process zones at the crack tip. In wood products the process zone is typically a fiber-bridging zone comprised of non-fractured constituent materials in the wake of a propagating crack tip. In MDF and DF, the fiber bridging consists of wood fibers that span the crack surface. In PB, it is wood particles. The zone can be small or large, but in wood products, the zone is generally large compared to typical lab-scale specimen dimensions. As a result, fiber bridging may influence the entire crack propagation process in lab-scale specimens.

The presence of fiber bridging complicates fracture experiments on wood products. First, such zones invalidate traditional fracture mechanics methods (*e.g.*, ASTM [2006] E399). Those methods rely on pre-calculated calibration functions to find toughness (*e.g.*, stress intensity factor) from failure load. Unfortunately, these functions assume stress-free fracture surfaces and thus are invalid for cracks with fiber bridging stresses. Second, fiber bridging can make it difficult to visually identify the crack tip and measure crack crack lengths; these lengths are needed for data reduction. Third, when fiber bridging is significant, the toughness increases as the crack propagates [Nairn 2009]. The fracture characterization of such materials requires continuous monitoring of toughness as a function of crack growth. The result is known as the material's *R* curve or fracture-resistance curve.

All fiber bridging issues can be overcome by available fracture mechanics methods, albeit, nonstandard ones. First, instead of using stress intensity methods requiring calibration functions, toughness can be measured using energy methods that find energy release rate directly from experiments even in the presence of bridging zones [Nairn 2009, Matsumoto and Nairn 2009]. The crack growth measurements needed for this method are made possible by measuring the strain field ahead of the crack tip using digital image correlation methods (DIC or full-field strain measurement techniques) [Sutton *et al*. 1983]. Shifts in this strain field with time imply an increment in crack growth [Matsumoto and Nairn 2009]. Finally, when applied to crack propagation experiments, these methods can measure the full *R* curve for the material [Matsumoto and Nairn 2009] rather the thus a single number.

The energy methods were used to measure the toughness during crack propagation for MDF, PB, and DF was measured. To study the role of resin, experiments were done of both conventiona resin and soy-resin PB. The resulting *R* curves were interpreted to derive toughness and bridging-effect information for each material. Because MDF, PB and DF are all anisotropic, the crack growth was characterized in different directions. In MDF and PB a crack plane perpendicular to the plane of the panel is called an in-plane crack (LT and TL), while a crack plane parallel to the plane of the panel is called an out-of-plane crack (ZL and ZT); see Fig. 1. In DF, a longitudinal crack with its plane perpendicular to the growth rings is a tangential-longitudinal crack (TL), while a crack with its plane tangential to the growth rings is a radial-longitudinal (RL) crack; see Fig. 1. All these crack orientations were studied. In general, the *R* curves started with some initiation toughness and then increased with crack length. The rate of increase was modeling by numerical methods [Nairn 2009] to calculate the bridging stress in the fiber-bridging zone.

MATERIALS AND METHODS

The MDF panels were provided by Flakeboard® (Springfield, OR) as 4 ft X 8 ft (T X L directions) panels at two densities, 609 and 737 kg/m^3 (38 and 46 lbs/ft^3) and in two thicknesses, 12.7 and 19.05 mm (0.5 and 0.75 in). Two types of PB were tested. One was a commercial PB with a urea formaldehyde (UF) resin (Roseburg Forest Products, Missoula pine particles, thickness 19.48 mm (0.767 in), and density 730 kg/m^3 (45.6 lbs/ft^3) purchased at local lumber store. The other was a research PB with a soy flour adhesive resin [Li *et al*. 2004] (thickness 19.43 mm (0.765 in), and density 653 kg/m^3 (40.8 lbs/ft^3). The solid wood specimens were select structural I Douglas fir free of knots (thickness 22.2 to 22.6 mm (0.866 in)). Prior to testing, all specimens were conditioned at 20˚C and 60% relative humidity until equilibrium.

All fracture tests used the modified compact tension (CT) specimens shown in Fig. 2. This specimen was derived from the standard CT specimen [ASTM 2006] except elongated in the width direction from 95.25 to 127.0 mm (3.75 to 5.0 in) to provide more room for crack propagation. The mode I loading was applied by steel pins at a constant displacement rate of 0.05 mm/min. The in-plane MDF, PB, and DF CT specimens were cut from panels or boards. Out-of-plane MDF and PB CT specimens were built up by gluing ZT or ZL orientation slices (see Fig 1) to arms cut from the main panel. By this method, all tests could be done with the same CT specimen geometry. The dashed lines in Fig. 2 indicate the location of the ZT or ZL slices for those specimens.

All fracture experiments were done using an energy-based method [Nairn 2009, Matsumoto and Nairn 2009]. This technique enables direct measurement of energy release rate during crack propagation and contains data analysis methods developed to reduce scatter. In brief, specimens were monotonically loaded while recording force and crack length as a function of displacement (Fig. 3A). While some crack propagation methods periodically unload the specimen to measure energy, that approach cannot be used for materials with fiber bridging because it crushes the fibers in the process zone and changes the results [Atkins and Mai 1985]. One option for measuring energy in materials with such crack plane interference is to assume unloading returns to the origin (if the process zone did not interfere). Indeed, recent experiments [Matsumoto and Nairn 2009] confirmed that this assumption is reasonable for MDF; here it was assumed reasonable for PB and DF as well. Thus, the cumulative energy released as function of displacement was measured by integrating the force-displacement curve up to each displacement and then subtracting the area under the assumed unloading curve (shaded area in Fig. 3A). Cross-plotting this measured energy (per unit thickness) with measured crack length gives cumulative energy released as a function of crack length (see Fig. 3B). Finally, the slope of this curve is the energy release rate as a function of crack length (the R curve); it was found by numerical differentiation (see Fig. 3C).

A key requirement of the energy method is accurate crack length measurement during the monotonic tests. For both MDF and PB, the crack tip was difficult to identify visually. This difficultly has led some researchers to define *effective* crack lengths [Ehart *et al*. 1996], but this approach, by definition, means the toughness will be *effective* property as well. Fortunately, crack lengths could be measured by using digital image correlation (DIC) [Sutton *et al*. 1983]. The specimens were painted with a speckle pattern. During crack propagation, a series of images were recorded. Analysis of these images using DIC methods resolved the axial strain in the path of the crack. The strain profiles were low far away of the crack tip, but became very high near the crack tip [Matsumoto and Nairn, 2009]. Although one cannot objectively identify the precise crack tip, these strain profiles retained their shape and simply shifted with the propagating crack. Using the shift in strain field between each image produced accurate measurements of crack growth increments. Crack length was determined by adding these increments to the initial crack length. The DIC methods were only needed for MDF and PB cracks. For DF, crack tips could be identified visually; these crack lengths were measured off digital images recorded during the tests.

Internal bond tests were conducted on both the commercial and soy PB panels following ASTM [2009b] D1037. The internal bond test is intended to determine the tensile strength perpendicular to the plane of the panel. Nine specimens of each type of panel were tested. Internal bond test results were compared to out-of-plane fracture toughness results (ZL and ZT crack growth) to assess each method as a tool for characterizing the quality of the internal bonds in the panel.

RESULTS

MDF

The MDF results are reported elsewhere [Matsumoto and Nairn 2009]. The experimental results are summarized here for comparison to PB and DF results and analyzed with new modeling (discussed below). The *R* curves for in-plane cracks (TL and LT) in the 19.05 mm thick MDF panels are in Fig. 4 (The 38 lbs/ft^3 LT directions could not be evaluated due to extremely curved cracks). The denser 46 lb/ft^3 (737 kg/m^3) panels had about twice the initial toughness of the 38 lbs/ft^3 (609 kg/m^3) panels. The initial toughness is defined as the start of the *R* curve or the toughness at the onset of crack growth. After initiation, the toughness increased almost linearly with crack length. The increase is caused by the development of a fiber-bridging zone. The initial specimen with the machined crack has no fiber bridging; as the crack propagates, a zone develops causing the toughness to increase with no indication of reaching a steady-state. In some materials, process zones reach a constant or steady state value and the *R* curve plateaus. In MDF, the toughness continues to increase, which implies the bridging zone continued to develop..

The dashed curves in plots are numerical models of crack propagation including fiber bridging, which are discussed below. Edge effects, which were common near the end of these tests, were an artifact of the data reduction scheme. The final toughness is determined from $R = dU/da$ were U is energy area and a is crack length (see Fig 3B). Near the end of the test, however, da approaches zero which causes R to become large and unreliable. All analyses here considered only data prior to these rapid rises.

The *R* curve results for LT cracks in thin (12.7 mm) MDF panels are given in Fig 5 and can be compared to results for thick (19.05 mm) panels in Fig. 4. Their initial MDF toughnesses were nearly independent of thickness for the range tested here. The thinner panel *R* curves, however, increased faster with crack growth, possibly because of a more effective process zone.

The *R* curve results for out-of-plane crack propagation in the ZL direction are shown in Fig. 6 (the results for ZT cracks were similar and are not plotted). Like in-plane cracks, the out-of-plane crack toughness rose linearly during crack growth and never reached steady state. In contrast, the initial toughness was about two orders of magnitude lower than in-plane toughness and is now relatively independent of panel density. Similarly, the magnitude of the increase in toughness with crack propagation is much lower indicating less effective fiber bridging. Wood fibers in MDF tend to lie in the plane of the panel and are therefore should be less effective at bridging out-of-plane cracks than in-plane cracks.

Particle Board

The *R* curves for in-plane crack propagation in both commercial and soy PB are shown in Fig. 7. The TL and LT directions were uncertain in these panels; these results are thus for generic in-plane cracks. The initial toughnesses for commercial and soy PB were similar, and were 2-3 times lower than that of MDF at a comparable density. Like MDF, PB toughness increased with crack length. Here the process zone is bridged by wood particles rather than wood fibers. Comparing commercial to soy PB, the commercial PB had a slightly higher initial toughness and its *R* curve reached a steady state (G_{ss}) of about 2030 J/m^2. The initial soy PB toughness was slightly lower, but the *R* curve continued to rise, never reaching a steady state prior to edge effects. The lower initial toughness of soy PB may be due to its lower density (653 kg/m^3 or 40.8 lbs/ft^3 for

the soy PB compared to 730 kg/m^3 or 45.6 lbs/ft^3 for the commercial). A slightly larger density difference in MDF panels had a significant effect on in-plane toughness.

The leveling off of toughness for commercial PB indicates a break down of the fiber-bridging zone. In commercial PB, the breakdown begins after about 40 mm of crack growth, which would equate to the length of the bridged zone. For subsequent crack growth, the bridging zone propagates along with the crack maintaining a nearly constant 40 mm length [Nairn 2009]. As a result, the R curve stays constant and equal to G_{ss} (see Fig. 7).

Compared to MDF, the out-of-plane crack propagation directions of PB (see Fig. 8) had higher toughness (1.5-7 times higher), especially for soy PB. These differences were attributed to their differing wood constituents and associated orientations. MDF uses wood fibers that tend to lie flat in the plane of the panel and provide little reinforcement in the z direction. In contrast, PB is composed of wood particles that are more three dimensional. As evidenced by crack propagation results, these particles bridge cracks better in the z direction than MDF fibers, which results in a higher toughness. Between soy and commercial PB, the soy PB toughness was about three times higher. Both PB R curves increased linearly at roughly the same rate. A three-fold increase in toughness could be due to the resin/wood particle bond differences.

Douglas Fir

Crack propagation results for Douglas fir are in Fig. 9. Douglas-fir had the lowest in-plane (RL and TL) fracture toughness of all materials tested. The initial toughnesses of the two crack propagation directions (RL and TL) were similar, but diverged with crack propagation. During crack propagation, TL direction toughness increased linearly with crack growth while the RL direction remained essentially constant. An increase with crack length in the TL direction can again be attributed to fiber bridging, but now the crack is bridged by non-fractured latewood zones. In contrast, an RL crack can find a path mostly through early wood, which apparently fractures with little material remaining to bridge the crack. This conclusion is supported by observations of the fracture surfaces. The TL fracture surface was rough with ridges at the latewood zones that had bridged the crack plane. In contrast, the RL fracture surface was very smooth because few wood fibers bridged the crack plane.

Internal Bond Tests

A common way to assess PB and resin quality is through the internal bond or IB test [ASTM 2009b]. In an IB test, a 2" by 2" block is glued to end blocks and loaded in transverse tension. To compare IB results to these new out-of-plane fracture results, IB tests were run on the same panels tested for fracture. The IB strength for the commercial PB was 0.43 MPa (62.4 psi) with coefficient of variation (COV) of 10.7%. For soy PB, the IB strength was 0.52 MPa (74.9 psi) with COV of 17.8%. The soy panel had a slightly higher value even with its lower panel density, but the relative difference between the two was small compared to the difference in their fracture toughness values. In other words, the PB results barely distinguish the two materials while the fracture results make a clear distinction that suggests the PB panels are significantly better — three times higher toughness.

CRACK PROPAGATION MODELING AND DISCUSSION

Fracture mechanics standards [ASTM 2006], and most prior work on wood (*e.g.*, [Schniewind and Centeno 1973, Johnson 1973]), emphasizes the fracture toughness at the initiation of crack

growth. In materials that develop process zones, this approach misinterprets the fracture properties of the materials. It discards all of the interesting effects that occur during crack propagation. For example, the initiation toughness in bone is exceedingly small, but its *R* curve rises rapidly during crack growth [Nalla *et al*. 2005]. Based on its initiation toughness, bone would be characterized as an unsuitable structural material. Fortunately, its full fracture behavior is much better.

Like bone, all wood composites and most solid wood fracture tested here had rising *R* curves. Since all curves were nearly linear in crack growth, the *R* curves can be described by an initiation toughness, G_{init}, and an *R* curve slope. The experimental results for these values are listed in Table 1. Only one crack path (RL fracture in DF) had zero slope. For most materials, the *R* curve continued to rise for the entire test, which suggests the potential bridging zone is large — larger than the specimen sizes used. Three materials appeared to reach a steady-state toughness: in-plane commercial PB and DF for both TL and RL fracture. The bridging toughness values for these materials are indicated in the Table 1. The bridging toughness is the difference between the steady-state toughness, G_{ss}, and initiation toughness, G_{init}, or $G_b = G_{ss} - G_{init}$.

To extract material properties from these data, the slopes should be interpreted in terms of the stresses carried by the bridging zone. This analysis requires numerical modeling of crack growth with fiber bridging, such as described in Nairn [2009]. The details are:

1. The CT specimens were discretized into material points using the material point method (MPM) [Sulsky *et al*. 1994] (see Fig. 10A). The particles were evenly spaced and separated by 0.635 mm (0.025 in) (this resolution verified for convergence). An initial crack was inserted using explicit crack methods for MPM [Nairn 2003]. The loading pins were modeled as steel cylinders and set to move at a constant velocity in the opening direction. Loads were transferred from the pins to the CT specimen by frictionless contact [Bardenhage *et al*. 2001, Lemial *at al*. 2010]. For in-plane cracks all material points in the specimen were the same. For out-of plane cracks, the material points in the center of the specimen were set to the properties of the *z*-crack slice, while the remaining particles used the in-plane properties for the same material.

2. At each time step, the *J* integral was calculated (by methods that account for the fiber-bridging zone [Nairn 2009]) and then compared to G_{init}, where G_{init} was determined from experiments. Whenever $J > G_{init}$, the crack tip propagated the distance of one particle spacing (0.635mm). In the wake of the crack propagation, a traction law was assigned between the two crack surfaces. The traction law was assumed to be linear softening (see Fig. 10B), in which the traction decrease linearly from the peak bridging stress, σ_b, to the critical COD, δ_c, where the fibers fail and the bridging zone starts to break down. The area under the traction law, $G_b = \sigma_b \delta_c /2$, is the total toughness associated with bridging. The linear softening law was selected, because it has been associated with linearly increasing *R* curves [Lindhagen and Berglund 2000, Nairn 2009].

3. The progressive failure analysis continued until the crack tip reached the end of the specimen. The *R* curve was calculated each time the crack propagated as $R = G_{init} + G_{b,released}$, where $G_{b,released}$, is the energy released by the entire bridging zone during the last increment in crack growth. This energy can be found from the shaded area under the traction law up to the current crack opening displacement at the opened edge of the bridging zone as indicated in Fig. 10B [Nairn 2009]. Finally, this *R* curve was output as a function of crack growth and

compared to experimental results. The traction law properties were varied until the modeling matched the experiments. Because few of the results reached steady state, the only traction law property that could be determined was σ_b, but it could be determined without needing to know G_b or δ_c.

The other mechanical properties necessary for simulations were also obtained from the fracture tests. The in-plane CT moduli were assumed to be isotropic and found by matching the experimentally observed specimen stiffness to a finite element calculation of that stiffness as a function of panel modulus. The panel parts of the out-of-plane CT specimens were also assumed isotropic and used the stiffness from the in-plane tests, but the cores (the central regions) were assumed to be transversely isotropic. The axial direction of the core was in the *y* direction and it represents the through-the-thickness modulus of MDF or PB. The modulus in the *x* direction was assumed to be the same as the panel modulus from the in-plane experiments. The axial shear modulus was assumed to be 2/3 the axial modulus. Thus, the only unknown modulus was the y direction modulus. It was found by matching the experimentally observed CT specimen stiffness to finite element calculations. Finally, DF was assumed to have typical orthotropic properties for DF [Bodig and Jayne 1982]. These values gave reasonable results for CT specimen stiffness. All assumed mechanical properties are given in Table 2. The resulting *R* curves are relatively insensitive to these specific values. The *R* curves depended much more on the assumed fracture properties and traction law properties.

All experimental results were fit to MPM modeling simulations to find σ_b; where possible, the fit also found G_b. The resulting fits are plotted in Figs. 4 to 9; the numerical results are in Table 1. The MPM results fit the simulations well, but had some noise. The noise is believed to be a consequence of dynamic fracture simulations. Whenever a computer simulation propagates cracks (by releasing elements in finite element analysis or by extending an explicit crack in MPM), the object will release energy. This propagation is meant to model crack propagation in real materials, but the real material absorbs that energy while creating the new surface area. In elastic simulations, however, there is no mechanism for absorbing the released energy. As a consequence the released energy becomes kinetic energy. This kinetic energy, which is localized at the crack tip, can induce oscillations in *J* integral calculations at the crack tip, which sometimes necessitate artificial damping. Here the oscillations were normally small and no damping was used. They were kept small by reducing the loading rate. All simulations used a loading rate of 1 m/sec, which is much faster then experiments, but small enough to avoid inertial effects and to minimize kinetic energy oscillations. The oscillations were similar in magnitude for out-of-plane cracks, but because the energy released was much smaller, they looked larger. Figure 6 shows one fit with all oscillations. The kinetic energy artifacts caused the simulated *R* curve to periodically overshoot the expected *R* curve for very short intervals (one or two time steps). The oscillations, however, were bounded on the bottom by the simulated *R* curve. Thus, for all out-of-plane simulations, the transient high points were removed and the plotted simulations are the envelope for the lower bound of the output results. The in-plane results plot the full *R* curves with all oscillations. Importantly, these oscillations have nothing to do with MPM. They are a natural consequence of any computational mechanics simulation that conserves energy while at the same time dynamically introduces crack extensions.

The bridging stresses for in-plane cracks in ~19 mm thick MDF 38, MDF 46, and PB (both resins) were 0.6 MPa, 0.8 MPa, and 1.0 MPa, respectively. A comparison of MDF 38 to MDF 46

shows that the denser panel had higher bridging stress, probably because the denser panel has more fibers per unit area. Comparing MDF to PB, PB had slightly higher bridging stress. The coarse particles in the center of PB are more effective at bridging than the fine fibers in MDF. For thinner panels (12.7 mm), the denser MDF 46 had higher bridging stress then MDF 38. Compared to thicker panels, the bridging stress for the thinner MDF panels was higher; it ranged from 1.1 to 4.0 MPa. Perhaps the manufacturing process of the thinner panels does a better job of aligning fibers in the plane of the panels. The better the fibers lie in the plane of a panel, the more effective they should be at bridging in-plane cracks.

The bridging stresses for out-of-plane cracks were all about an order of magnitude lower than for in-plane cracks. Apparently the panel structure promotes bridging of in-plane cracks but inhibits bridging of out-of-plane cracks. For MDF, in particular, the predominantly in-plane fibers will be parallel to out-of-plane cracks and thus very ineffective at carrying a bridging stress. As with in-plane cracks, the bridging stress for out-of-plane cracks in PB was higher than for MDF for likely the same reasons.

Because the crack propagation rarely reached steady state, the only traction law parameter that could be measured was the bridging stress. Although neither G_b nor δ_c could be measured, those properties can be bounded. The G_b column in Table 1 has an lower bound to G_b calculated from maximum observed R value prior to edge effects. This result is a lower bound because the actual G_b would be higher if the crack propagation could have been extended to steady state. By using the relation $G_b = \sigma_b \delta_c/2$, a lower bound for G_b leads to a lower bound for the bridging COD: $\delta_c \geq 2G_b/\sigma_b$; the results are in Table 1. For in-plane cracks δ_c is about 1 to 2 mm, which is similar to the dimensions of wood elements (*e.g.*, longitudinal tracheids [Bowyer et al. 2000] or particles) in MDF or in PB and reinforces the argument that the rising R curve is related to bridging of these elements across the crack surface. The critical COD for the out-of-plane cracks are less than 1 mm. One interpretation is that the fibers or particles tend to lie closer to the plane of the panel and thus are easier to pull out in the thickness direction.

The crack plane for out-of-plane fracture tests is the same as the failure plane in IB tests. As a consequence, the out-of-plane fracture tests might be a candidate for a new test that can replace IB testing. Most areas of material science identify fracture toughness as a more fundamental material property [Williams, 1984]. IB tests were run on the same PB panels tested by crack propagation. The IB results suggest that the commercial and soy panels are of similar quality (producing similar failure stresses within similar COVs), while the fracture results suggest that the soy resin panel is significantly better. Unfortunately, no COV for the fracture tests could be assessed (since only one test was done for each material due to it's time consuming nature). In general, however, fracture tests have less scatter than strength tests. In fracture tests the crack is forced to propagate from a well-controlled crack tip. In strength tests, the failure occurs at statistically random locations resulting in much higher scatter. Furthermore, a single fracture test (as done here) gives a full R curve and thus represents more information than a single value obtained in other tests. The question remains: Which test is a better measure of quality? Can fewer, but more time consuming fracture tests, lead to better products than many highly-scattered IB tests? The results here suggest that out-of-plane fracture testing might identify differences in panels that are not evident in IB testing. Those differences might translate to improved panels if used to guide new materials development.

The DF fracture results showed a dramatic difference between TL and RL fracture, but that difference is only observed by monitoring crack propagation. Most prior fracture work on DF (and some other species) has focused on initiation. The results vary and the interpretations are misguided because they are based on incomplete fracture information. Two prior initiation studies used conventional fracture methods to measure critical stress intensity factors, K_{Ic}, for both TL and RL fracture of DF. Schniewind, and Centeno [1973] found K_{Ic} of 0.409 MPa √m for RL fracture and 0.309 MPa √m for TL fracture. They concluded the differences were significant and "could be attributed to rays acting as crack arrestors in the RL system, while in the TL system the cracks can run along the rays." Johnson [1973] found K_{Ic} of 0.324 MPa √m for RL fracture and 0.374 MPa √m for TL fracture. Here the ranking of TL and RL toughness was switched, but they concluded the fracture properties for these two directions were indistinguishable.

To compare with these prior results, the K_{Ic} results were converted to energy release rates. The conversion for orthotropic materials [Kanninen and Popelar 1985] is:

$$G_{Ic} = \frac{K_{Ic}^2}{E_{eff}} \tag{1}$$

where the effective modulus, E_{eff}, depends on the crack plane. For RL fracture:

$$\frac{1}{E_{eff}} = \sqrt{\frac{1}{2E_{LL}E_{RR}}}\left(\sqrt{\frac{E_{LL}}{E_{RR}}} + \frac{E_{LL}}{2G_{LR}} - \nu_{LR}\right)^{1/2} \tag{2}$$

For TL fracture:

$$\frac{1}{E_{eff}} = \sqrt{\frac{1}{2E_{LL}E_{TT}}}\left(\sqrt{\frac{E_{LL}}{E_{TT}}} + \frac{E_{LL}}{2G_{LT}} - \nu_{LT}\right)^{1/2} \tag{3}$$

Using the DF properties in Table 2, the E_{eff} for RL and TL fracture are 1507 MPa and 1135 MPa, respectively. The Schniewind and Centeno [1973] results for G_{Ic} are 111 J/m^2 for RL fracture and 84 J/m^2 for TL fracture. The Johnson [1973] results for G_{Ic} are 70 J/m^2 for RL fracture and 123 J/m^2 for TL fracture. These results are similar to initiation values measured by the energy method, but the propagation results show that TL is tougher. This new fracture information shows that ray cells play little or no role in DF fracture. The ray cells are certainly neither arresting nor bridging the RL fracture surface.

Two other studies used wedge specimens and found toughness from work of fracture or total area under the load deflection curve (although for species different than DF) [Fruhmann *et al*. 2002, Reiterer *et al*. 2002a, 2002b]. In theory, this approach measures an average toughness that includes the effects of crack propagation. It is uncertain, however, how it might be influenced by specimen shape or edge effects. Furthermore, they measured only a single toughness rather than a full *R* curve. The findings of these two studies differed. Frühmann *et al*. [2002] found the TL toughness higher than the RL toughness in both spruce and beech. They concluded that latewood material enhanced the TL toughness. Reiterer *et al*. [2002a, 2002b] observed RL toughness higher than TL toughness in spruce, alder, oak and ash. They attributed the difference to ray cells, particularly in the hardwood species. Like initiation methods, the interpretation of total

fracture work as a single toughness ignores much of the fracture information. An average toughness, at best, is a sum of initiation and the average bridging toughness over the length of the specimen. No specific fiber bridging properties are measured. The full characterization of the fracture toughness of solid wood or wood composites should always monitor toughness as a function of crack growth. Differences between species, crack planes, or wood products should be based on this full *R* curve instead of the partial information provided by other tests.

REFERENCES

ASTM (2006) Standard Test Method for Plane-Strain Fracture Toughness of Metallic Materials. ASTM Designation: E399-05a.

ASTM (2009a) Standard Test Methods for Structural Panels in Flexure. ASTM Designation: D 3043-00.

ASTM (2009b) Standard Test Methods for Evaluating Properties of Wood-Base Fiber and Particle Panel Materials. ASTM Designation: D 1037-06a.

Atkins AG, Mai YW (1985) Elastic and Plastic Fracture. John Wiley & Sons, New York.

Bardenhagen SG, Guilkey JE, Roessig KM, Brackbill JU, Witzel WM, Foster JC (2001) An improved contact algorithm for the material point method and application to stress propagation in granular material. *Computer Modeling in Engineering & Sciences* **2**:509–522.

Bodig, J, Jayne BA (1982) Mechanics of Wood and Wood Composites. Van Nostran-Reinhold Co, Inc., New York.

Bowyer JL. Shmulsky R, Haygreen JG (2007) Forest Products & Wood Science, An Introduction, Fifth Edition. Blackwell Publishing, Ames, Iowa, USA.

Ehart RJA, Stanzl-Tchegg SE, Tschegg EK (1996) Characterization of Crack Propagation in Particleboard. *Wood Science and Technology* **30**:307–321.

Fruhmann K, Reiterer A, Tschegg EK, Stanzl-Tschegg SS (2002) Fracture Characteristics of Wood Under Mode I, mode II and mode III loading. *Philosophical Magazine A: Physics of Condensed Matter, Structure, Defects and Mechanical Properties* **82**(17-18):3289–3298.

Johnson JA (1973) Crack initiation in wood plates. *Wood Science* **6**(2):151–158.

Kanninen MF, Popelar CH (1985) Advanced Fracture Mechanics. Oxford University Press, New York. 41 pp.

Lemiale V, Nairn JA, Hurmane A (2010) Simulation of Equal Channel Angular Pressing with the Material Point Method. *Computer Modeling in Engineering & Sciences*, submitted

Li K, Peshkova S, Geng X (2004) Investigation of Soy Protein-Kymene Adhesive Systems for Wood Composites. *J. Am. Oil Chem. Soc.* **81**(5):487-491.

Lindhagen JE, Berglund LA (2000) Application of Bridging-Law Concepts to Short-Fibre Composites Part 1: DCB Test Procedures for Bridging Law and Fracture Energy. *Comp. Sci. & Tech.* **60**:871–883.

Matsumoto N, Nairn JA (2009) The Fracture Toughness of Medium Density Fiberboard (MDF) Including the Effects of Fiber Bridging and Crack-Plane Interference. *Engr. Fract. Mech.* **76**:2748-2757.

Nairn JA (2003) Material point method calculations with explicit cracks. *Computer Modeling in Engineering & Sciences* **4**:649–664.

Nairn JA (2009) Analytical and Numerical Modeling of R curves for Cracks with Bridging Zones. *Int. J. Fracture* **155**:167-181.

Nalla RK, Kruzic JJ. Kinney JH, Ritchie RO (2005) Mechanistic aspects of fracture and R-Rurve behavior in human cortical bone. *Biomaterials* **26**(2):217-231.

Reiterer A, Sinn G, Stanzl-Tschegg S (2002a) Fracture Characteristics of Different Wood Species Under Mode I Loading Perpendicular to the Grain. *Materials Science and Engineering A* **332**(1-2):29–36.

Reiterer A, Burgert I, Sinn G, Tschegg S (2002b) The radial reinforcement of the wood structure and its implication on mechanical and fracture mechanical properties - a comparison between two tree species. *Journal of Materials Science* **37**(5):935–940.

Schniewind AP, Centeno JC (1973) Fracture Toughness and Duration of Load Factor I. Six Principal Systems of Crack Propagation and the Duration Factor for Cracks Propagating Parallel to Grain. *Wood Fiber* **5**:152–159.

Sulsky D. Chen Z, Schreyer HL (1994) A Particle Method for History-Dependent Materials. *Comput. Methods. Appl. Mech. Engrg.* **118**:179–186.

Sutton MA, Wolters WJ, Peters,WH, Rawson WF, McNeil SR (1983) Determination of Displacement Using an Improved Digital Image Correlation Method. *Image and Vision Computing* **1**(3):133-139.

Williams JG (1984) Fracture Mechanics of Polymers. John Wiley & Sons, New York.

ACKNOWLEDGEMENTS

This work was support, in part, by a grant from the US Department of Agriculture, Cooperative State Research, Education, and Extension Service (2008-35504-19227)

Table 1: Experimental and simulation results for fracture properties of MDF, PB, and DF. G_{init} and R slope come from experimental results; σ_b are results of the simulations; G_b and δ_c are bounds on those properties based on experimental and simulation results (if listed with ">") or measured value (if listed with "=")

Material	Crack	Thickness (mm)	G_{init} (J/m²)	R Slope (J/m²/mm)	σ_b (MPa)	G_b (J/m²)	δ_c (mm)
MDF 38	LT	19.05	2230	10.00	0.60	>450	>1.5
	LT	12.70	2048	19.60	1.10	>1182	>2.2
	Z	19.05	59	0.35	0.06	>16	>0.5
	Z	12.70	52	0.25	0.04	>12	>0.6
MDF 46	LT	19.05	4550	18.00	0.80	>650	>1.6
	TL	19.05	4450	18.00	0.80	>750	>1.9
	LT	12.70	4150	60.00	2.00	>1950	>2.0
	TL	12.70	4000	60.00	4.00	>3000	>1.5
	Z	19.05	48	0.22	0.04	>11	>0.5
	Z	12.70	82	0.26	0.04	>12	>0.6
PB Comm	LT/TL	19.48	1460	16.60	1.00	=570	=1.2
	Z	19.48	120	0.72	0.10	>31	>0.6
PB Soy	LT/TL	19.43	1330	14.20	1.00	>490	>1.0
	Z	19.43	300	1.25	0.10	>45	>0.9
DF	TL	22.23	215	6.10	0.80	=405	=1.0
	RL	22.60	158	0.09	0.00	=0	=0

Table 2: The mechanical properties calculated from CT specimens and used in all plotted simulations. For isotropic properties, the E column gives the modulus. For transversely isotopic Z slices, E gives the modulus in the x direction; the y direction modulus, axial direction is given in the E_A column.. For DF, E gives the longitudinal modulus and the other columns give all other orthotropic properties.

Material	**Thickness (mm)**	**E (MPa)**	**E_A (MPa)**	**G (MPa)**	**ν**
MDF 38	19.05	1350			
MDF 38	12.7	1185			
MDF 38 Z	19.05	1350	90	$G_A = 60$	$\nu_A = 0.1$
					$\nu_T = 0.33$
MDF 46	19.05	2190			
MDF 46	12.7	2600			
MDF 46 Z	19.05	2190	200	$G_A = 100$	$\nu_A = 0.1$
					$\nu_T = 0.33$
PB Comm	19.48	1785			
PB Comm Z	19.48	1785	220	$G_A = 140$	$\nu_A = 0.1$
					$\nu_T = 0.33$
PB Soy	19.43	2016			
PB Soy Z	19.43	2016	90	$G_A = 55$	$\nu_A = 0.1$
					$\nu_T = 0.33$
DF	22.23	14500	$E_{RR} = 960$	$G_{LR} = 830$	$\nu_{LT} = 0.42$
			$E_{TT} = 620$	$G_{LT} = 760$	$\nu_{LR} = 0.37$
				$G_{RT} = 80$	$\nu_{TR} = 0.35$

FIGURE LEGENDS

1. Crack planes in MDF and PB (left) and in DF (right). Each crack is defined by two letters. The first letter is the direction normal to the crack plane; the second letter is the direction of crack propagation.
2. The elongated compact tension specimens used for all fracture experiments. All dimensions are in inches. The specimens were loaded by 0.75 in steel pins in displacement control.
3. Energy method for measuring *R* curve during crack propagation. A. The experiment is to measure force and crack length as a function of displacement. B. The shaded cumulative energy area (per unit thickness) is then cross plotted as a function of crack length. C. The *R* curve is slope of that energy plot found by numerical differentiation.
4. The fracture toughness of two different density MDF panels (19.05 mm thick) for in-plane cracks. The dashed line are a numerical model for crack propagation including fiber bridging.
5. The fracture toughness of two different density MDF panels (12.7 mm thick) for in-plane cracks. The dashed lines are a numerical model for crack propagation including fiber bridging.
6. The fracture toughness of two different density and two different thickness MDF panels for out-of-plane ZL cracks. The dashed lines are a numerical model for crack propagation including fiber bridging.
7. The fracture toughness for in-plane cracks in PB with two different resins. The dashed lines are a numerical model for crack propagation including fiber bridging.
8. The fracture toughness for out-of-plane cracks in PB with two different resins. The dashed lines are a numerical model for crack propagation including fiber bridging.
9. The fracture toughness for TL and RL cracks in Douglas fir. The dashed line is a numerical model for crack propagation including fiber bridging.
10. A. MPM model for CT specimens. The dark line in the middle is the initial crack. The round pins are steel. The central area is identical to rest of panel for in-plane cracks, but has Z-slice properties for out-of-plane cracks. B. A pure linear-softening traction law, which is linear from peak bridging stress, σ_b, to critical crack opening displacement, δ_c.

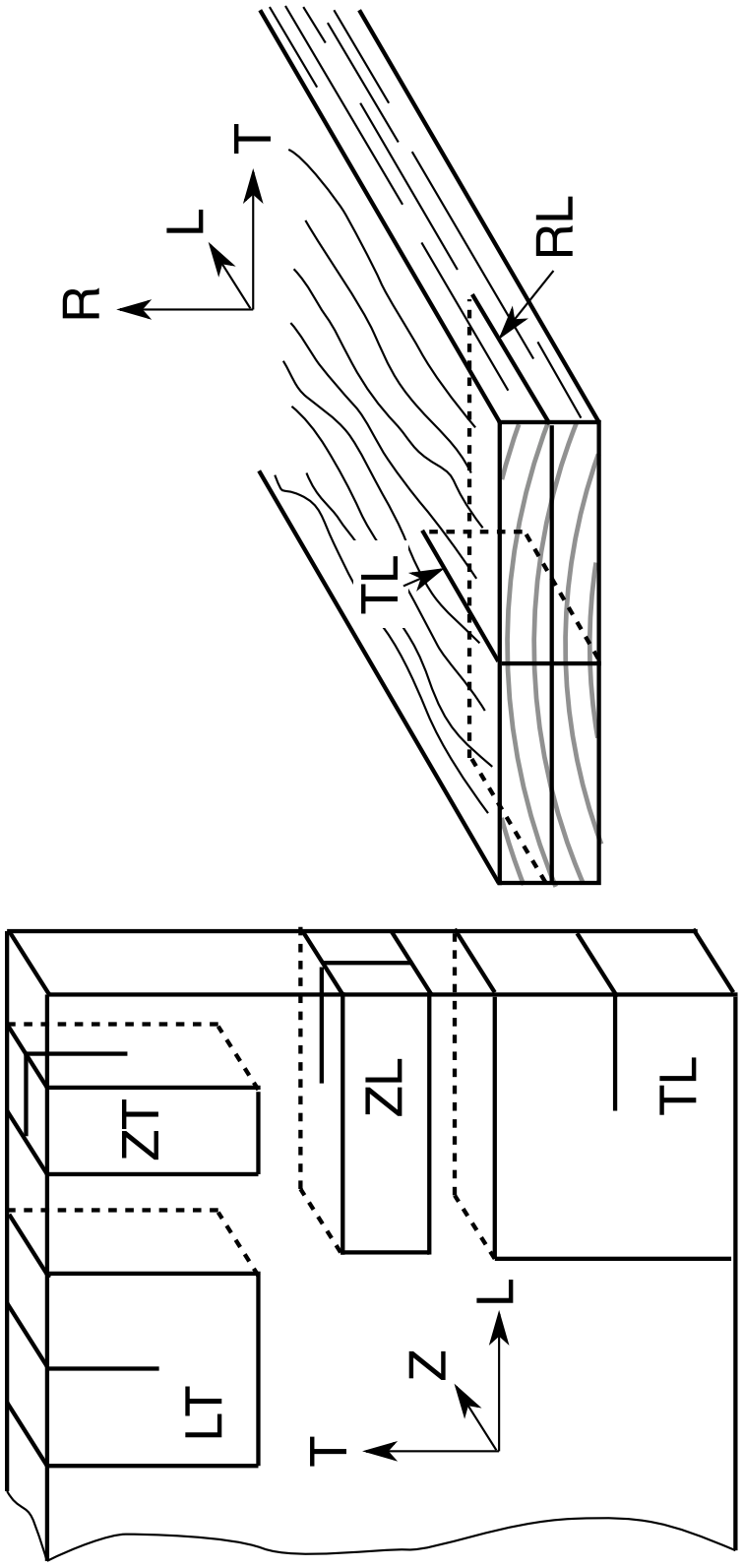

Figure 1

Figure 2

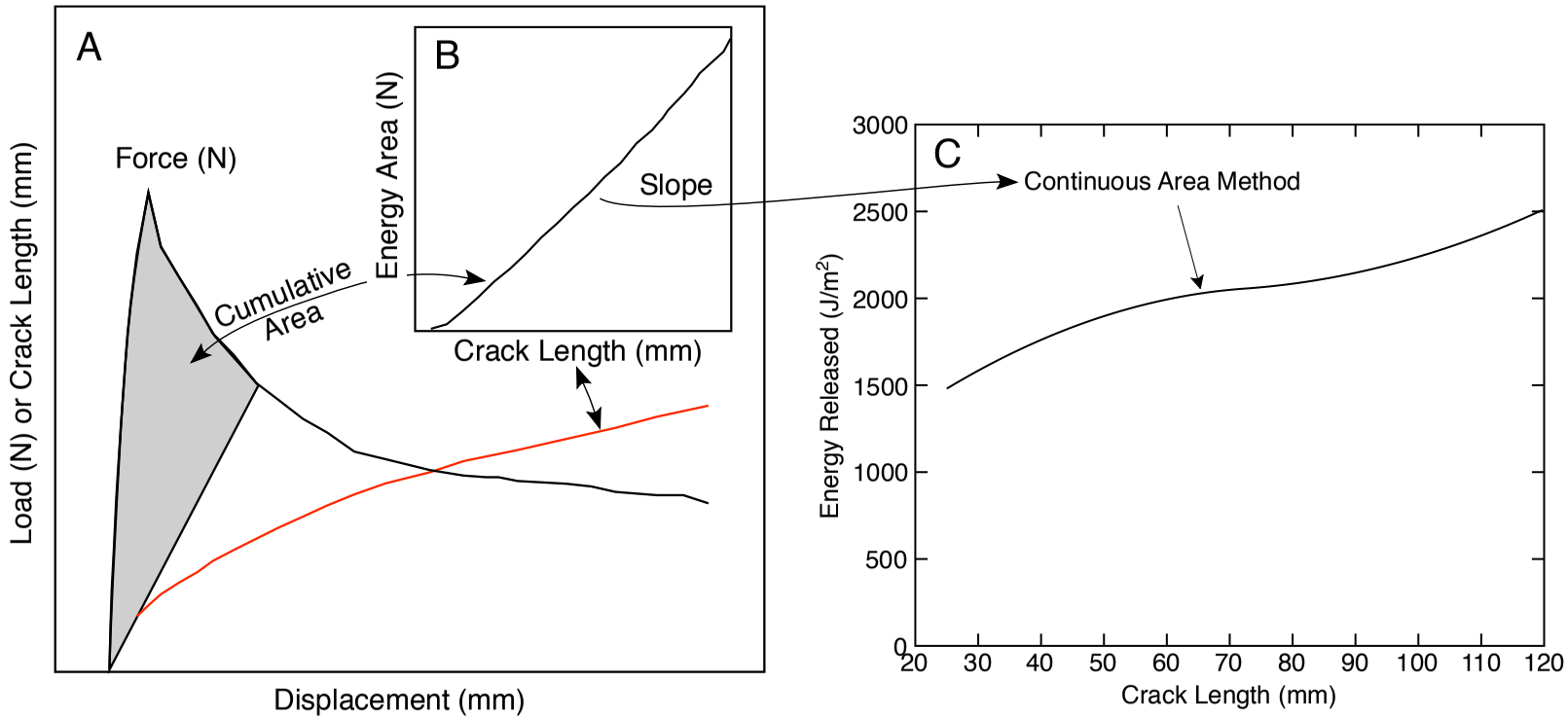
A
Force (N)
Cumulative Area
Load (N) or Crack Length (mm)
Displacement (mm)
B
Energy Area (N)
Slope
Crack Length (mm)
C
Continuous Area Method
Energy Released (J/m2)
3000
2500
2000
1500
1000
500
0
20
30
40
50
60
70
80
90
100
110
120
Crack Length (mm)

Figure 3

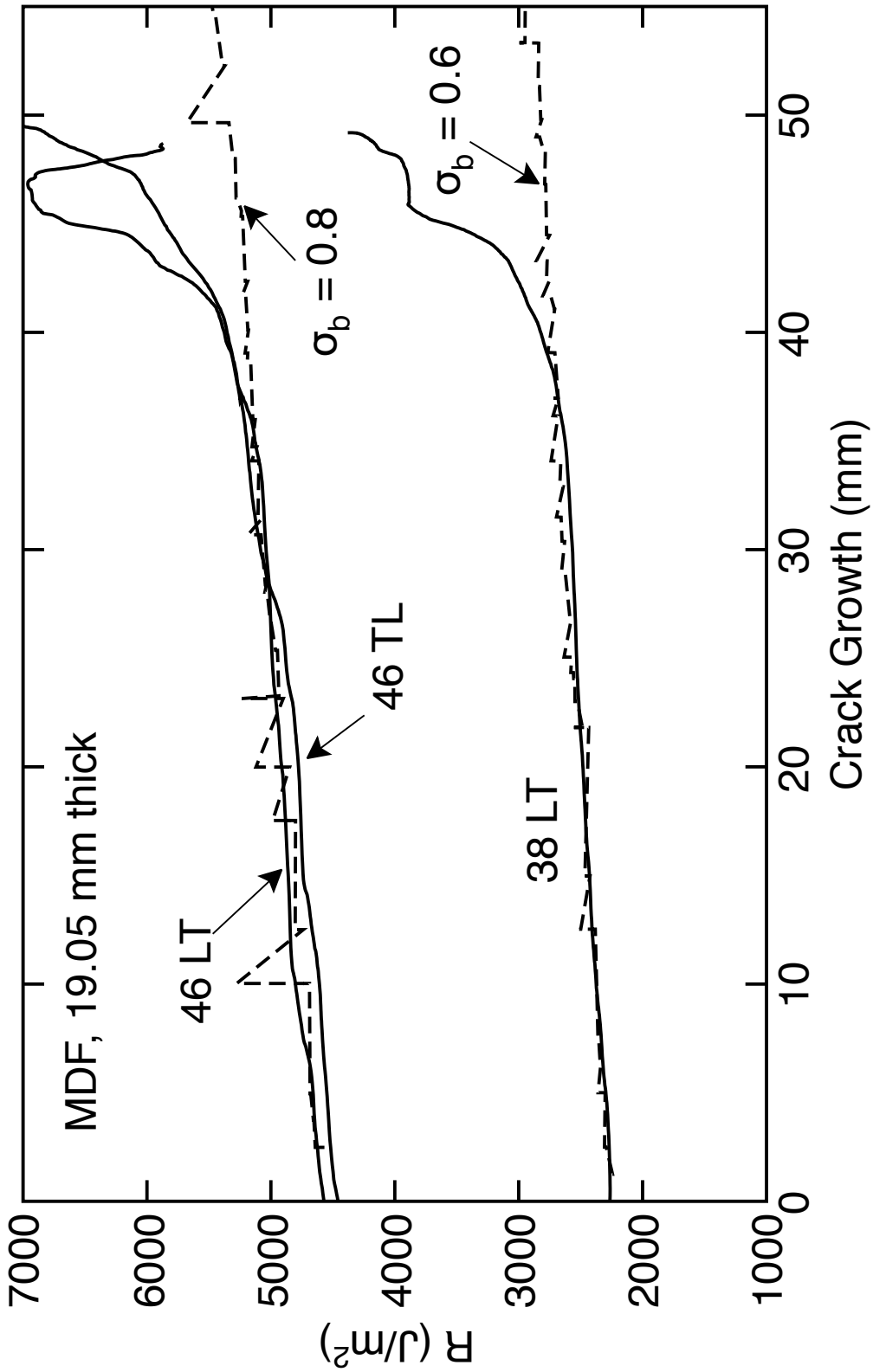
MDF, 19.05 mm thick
46 LT
46 TL
38 LT
$\sigma_b = 0.8$
$\sigma_b = 0.6$
R (J/m²)
Crack Growth (mm)
7000
6000
5000
4000
3000
2000
1000
0
10
20
30
40
50

Figure 4

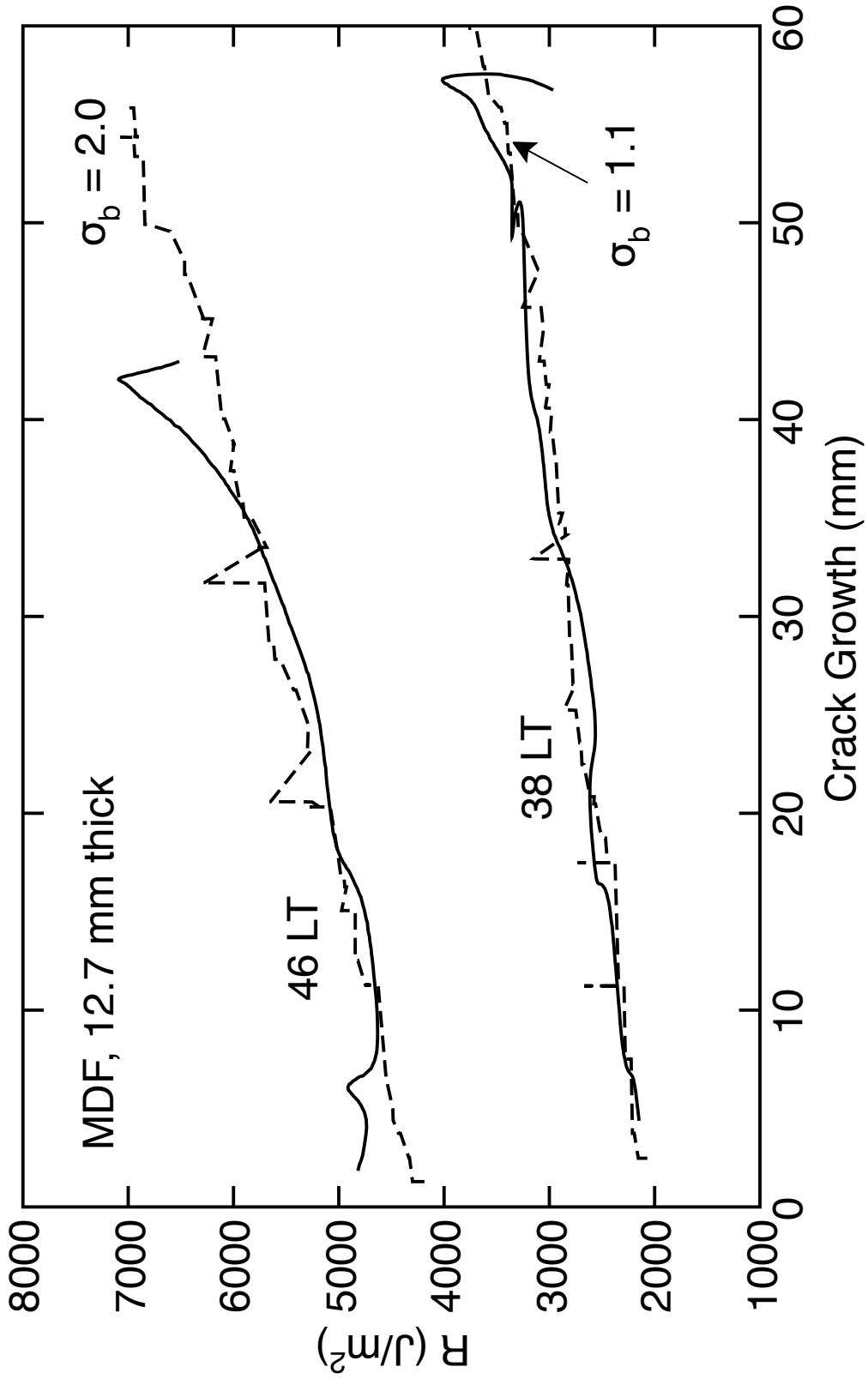
MDF, 12.7 mm thick
σ_b = 2.0
σ_b = 1.1
46 LT
38 LT
R (J/m^2)
Crack Growth (mm)
8000
7000
6000
5000
4000
3000
2000
1000
0
10
20
30
40
50
60

Figure 5

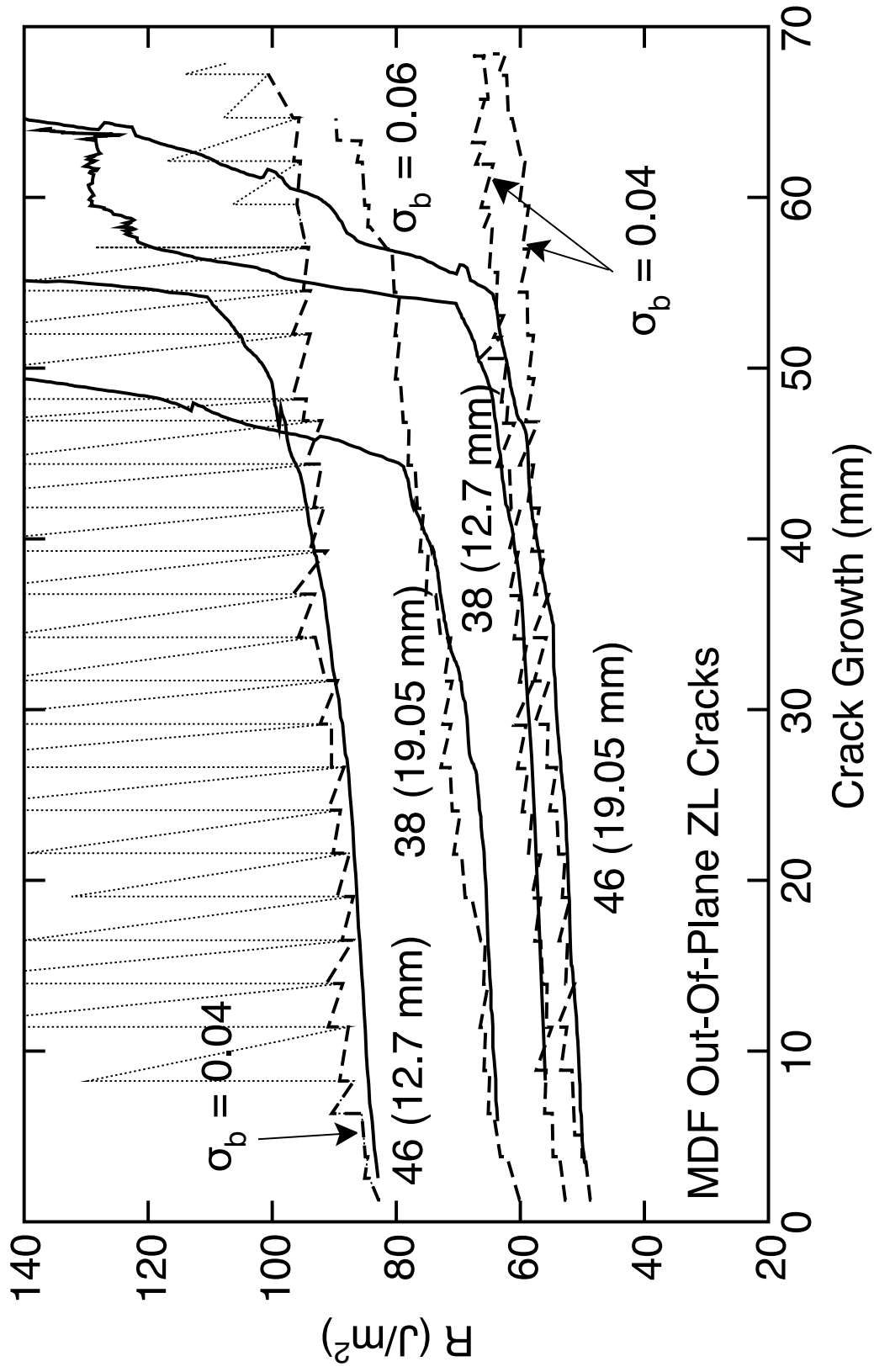
R (J/m²)
Crack Growth (mm)
MDF Out-Of-Plane ZL Cracks
σb = 0.04
σb = 0.06
σb = 0.04
46 (12.7 mm)
38 (19.05 mm)
38 (12.7 mm)
46 (19.05 mm)
20
40
60
80
100
120
140
0
10
20
30
40
50
60
70

Figure 6

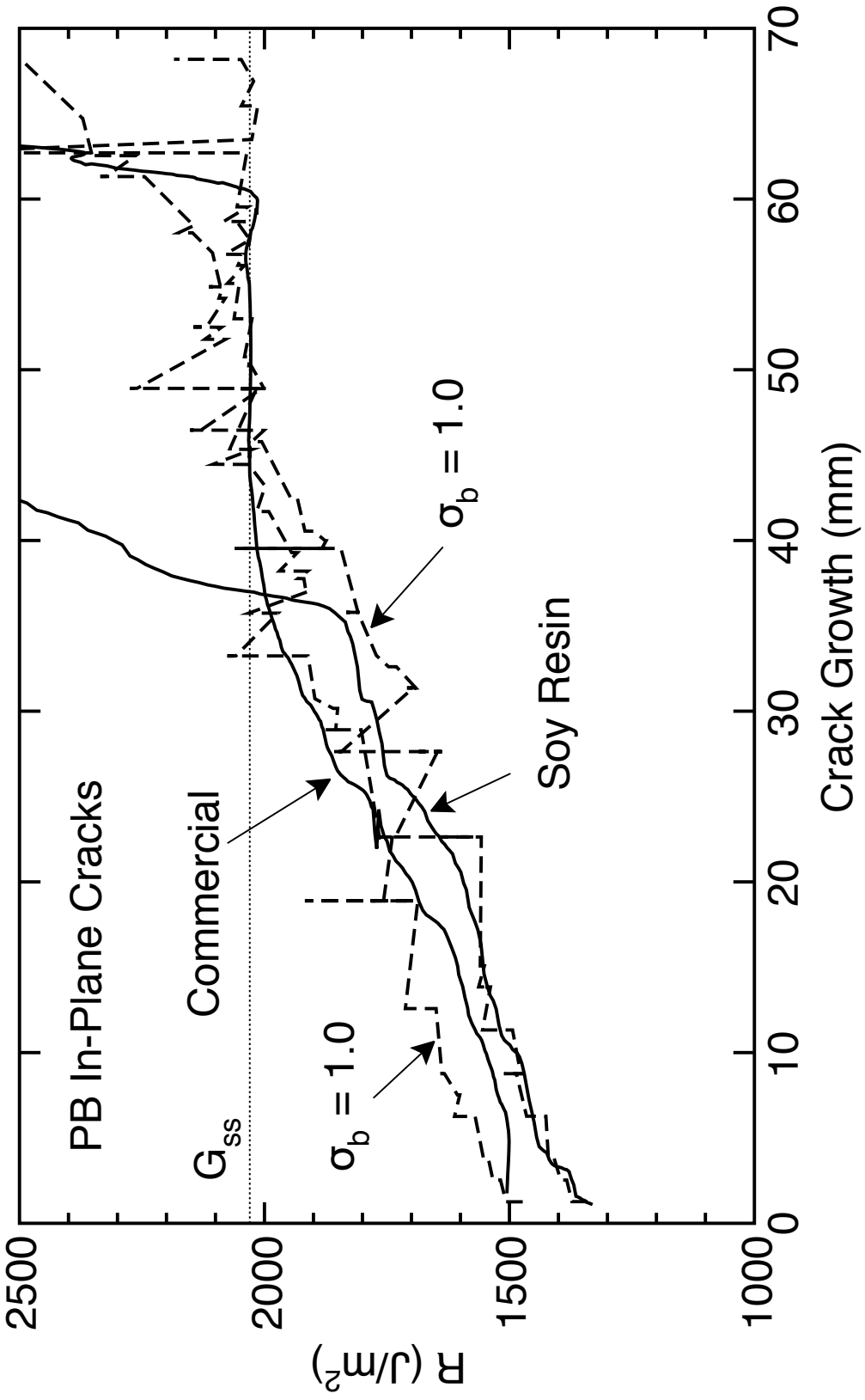
PB In-Plane Cracks
Commercial
Soy Resin
G_{ss}
σ_b = 1.0
σ_b = 1.0
R (J/m^2)
Crack Growth (mm)
2500
2000
1500
1000
0
10
20
30
40
50
60
70

Figure 7

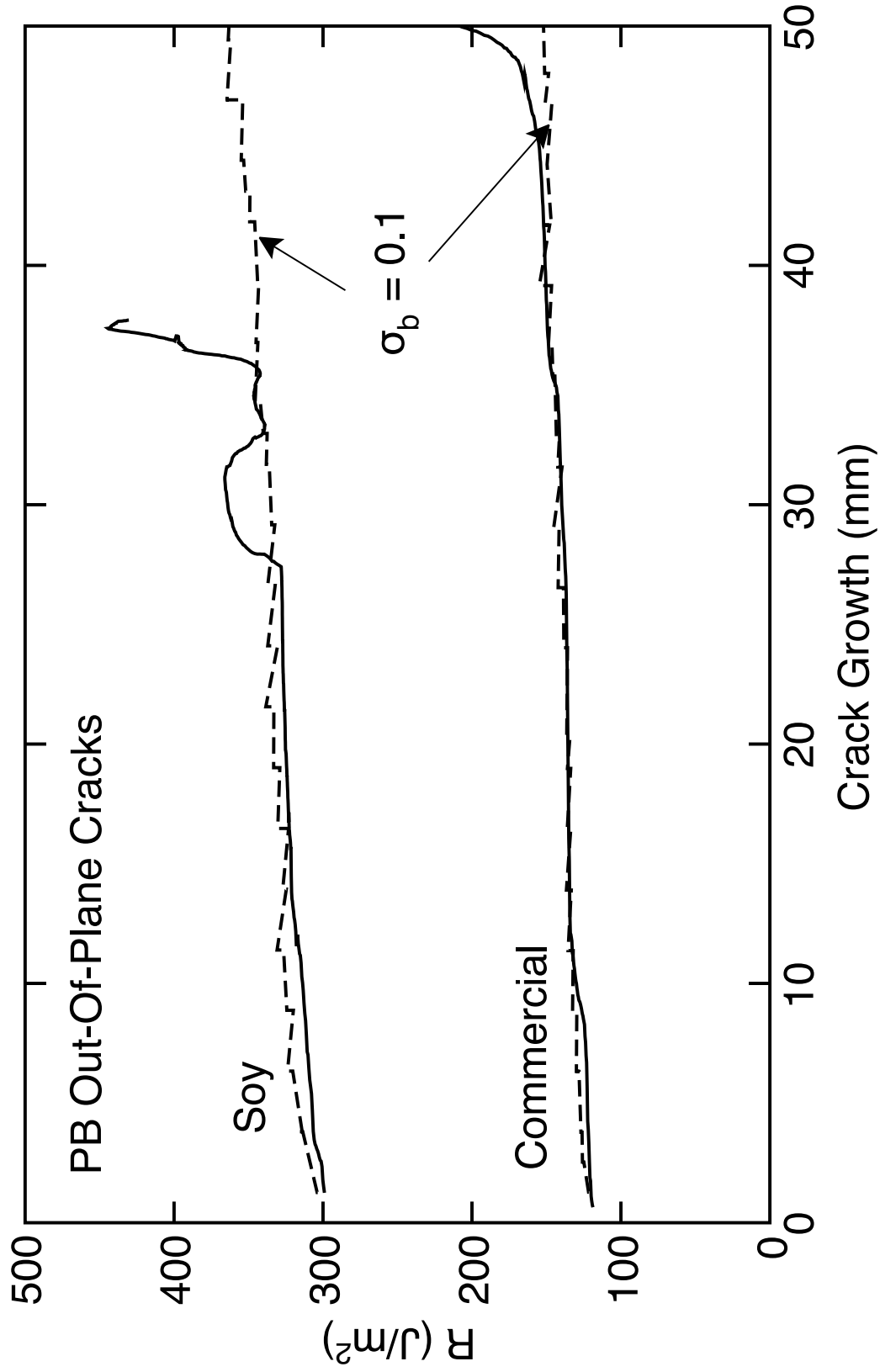
PB Out-Of-Plane Cracks
Soy
Commercial
$\sigma_b = 0.1$
R (J/m²)
Crack Growth (mm)
0
100
200
300
400
500
0
10
20
30
40
50

Figure 8

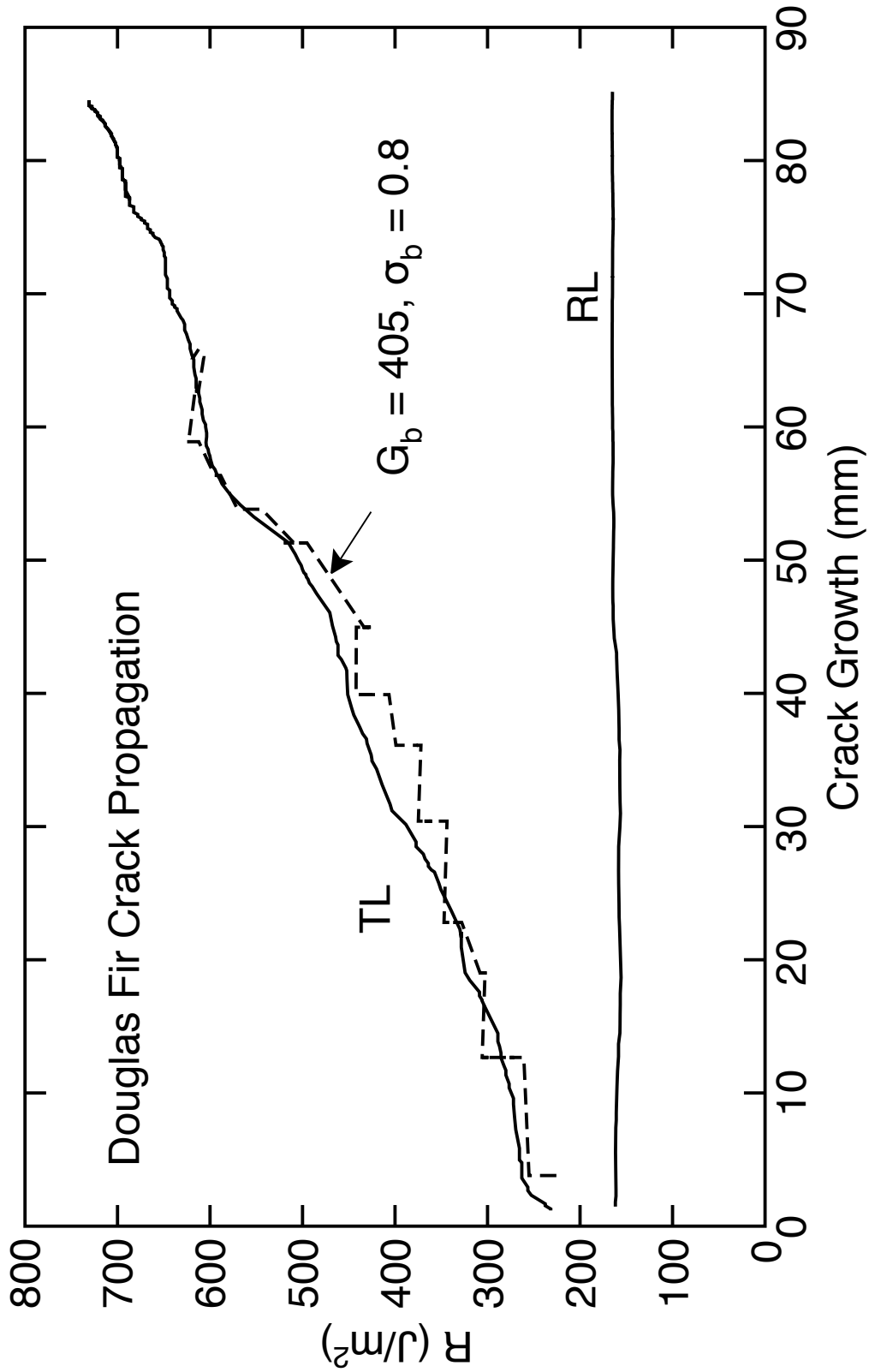
Douglas Fir Crack Propagation
TL
RL
G_b = 405, σ_b = 0.8
R (J/m^2)
Crack Growth (mm)
0
100
200
300
400
500
600
700
800
0
10
20
30
40
50
60
70
80
90

Figure 9

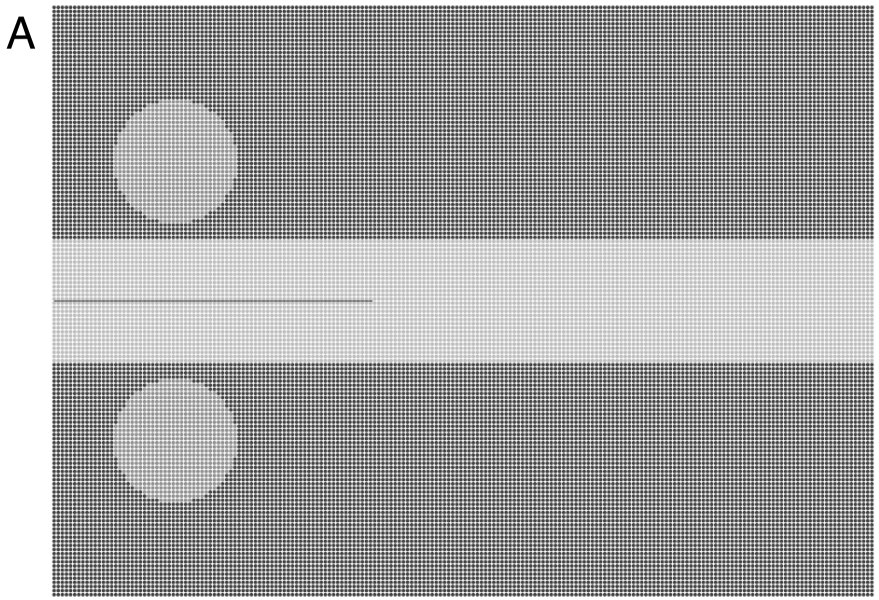

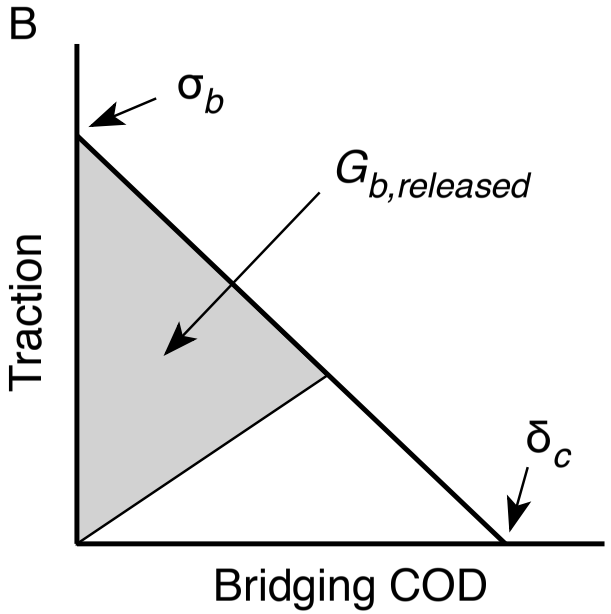

Figure 10